

Temporal Instability of Confined Viscoelastic Swirling Liquid Film with High-speed Compressible Gas

Huanran Wang^{1*}, Zhaoyu Liu¹, Hongjie Wang¹, Yafei Guo¹, Bingyang Liu¹, Yue Li¹, Shang Zhang¹ and Xuyang Liu¹

¹ Xi'an Aerospace Propulsion Institute, Shaanxi 710100, China

*Corresponding Author: zy1715212@buaa.edu.cn

Abstract: The linear instability of a confined viscoelastic liquid film with central compressible gas is theoretically investigated in this study. And the heat and mass transfer is also considered. The dispersion relation including both heat and mass transfer and gas compressibility is obtained. The heat and mass transfer is characterized by the ratio between the conduction heat flux and evaporation heat flux, and the gas compressibility is characterized by the gas Mach number. The results suggest that both the maximum growth rate and unstable wavenumber range increase as the ratio of the conduction heat flux to evaporation heat flux increases. The gas Mach number has a destabilizing effect on the gas-liquid interface. However, its effect is neglectable when the gas Mach number is small. Increasing the gas-liquid density can promote the breakup process. Furthermore, the effect of viscoelasticity of liquid phase is also examined. The stress relaxation time has an unstable effect on the gas-liquid interface, and the increasing deformation retardation time plays a stabilizing role. And the effects of Weber number, Reynolds number and other dimensionless parameters are also studied.

Keywords: viscoelastic liquid film; compressible gas; heat and mass transfer; Kelvin-Helmholtz instability; atomization.

Nomenclature

$\frac{A}{r}$	amplitude of oscillation	U_l	basic velocity of liquid in the axial direction
A_1	undetermined coefficient	u	perturbed velocity in axial direction
A_2	undetermined coefficient	V	velocity in axial direction
B_1	undetermined coefficient	v	perturbed velocity in radial direction
B_2	undetermined coefficient	v_g	perturbed velocity of gas in radial direction
h	disturbance wavelength	v_l	perturbed velocity of liquid in radial direction
K	dimensionless wavenumber	W	velocity in azimuthal direction
k	wavenumber	w	perturbed velocity in azimuthal direction
k_g	gas thermal conductivities	γ	liquid-to-gas velocity ratio
k_l	liquid thermal conductivities	θ	azimuthal angle
L	latent heat	Λ	ratio between conduction heat flux from wall to interface and the evaporation heat flux at the interface
Nu	Nusselt number of gas	ρ	gas-to liquid density ratio
n	azimuthal wave number	ρ_g	gas density
p	perturbed pressure	σ	surface tension coefficient of liquid
p_g	perturbed pressure of gas	Ω	dimensionless complex frequency
p_l	perturbed pressure of liquid	ω	complex frequency
Ro	Rosby number of liquid		
T_i	temperature at the liquid-gas interface		
T_g	temperature of gas		
T_w	temperature at wall		
t	time		
ρ_l	liquid density		
U	velocity in axial direction		
U_g	basic velocity of liquid in the axial direction		

1 Introduction

The air-assist or air-blast atomizers have been widely used in various combustion applications such as liquid rocket engines, gas turbines, aero engines and so on. The mean droplet size, mainly depending on the development of the gas-liquid interface disturbance, has remarkable influence on the combustion instability and efficiency (Eggers and Villermaux 2008). Rayleigh (1878) first used the linear stability theory to study the instability of liquid jet, and the theoretical results obtained by Rayleigh (1878) agree well with experimental results (Lafrance 1975). Reitz and Bracco (1982) studied the stability of a high-speed liquid jet injected through a circular nozzle into an initially stagnant gas. They obtained the zero-order dispersion relationship, and discussed the jet atomization phenomenon using appropriate experimental apparatus. The instability of a viscous liquid jet injected into an inviscid gas medium was investigated, and the zero-order and n-order dimensionless dispersion equation were obtained (1995). Zhang (2018) studied the breakup process of liquid jet in incompressible airflow, and showed that surface wave can cause instability of the jet column, big droplet of bag breakup and about 60 μm diameter droplet of shear breakup. In addition, the effect of surfactant-laden (Dharmendra and Gaurav Sharma 2018; Hu et al. 2018) and thermal effects on the surface tension (Hu et al. 2016; 2017; 2018) were also taken into consideration. Yang (2019) studied the effects of liquid-gas momentum ratio on atomization characteristics of internal mixing gas-liquid injector.

Viscous potential theory has been used to analyze the capillary and Kelvin-Helmholtz (K-H) instability of a viscous liquid jet surrounded by a viscous gas (Funada and Joseph 2001; Wang et al. 2004). Moreover, Funada et al. (2004) presented a detailed viscous potential flow analysis for the K-H instability at the interface of air above a liquid in a channel. And the potential flow theory was introduced to investigate the K-H instability of the viscoelastic liquid film (Fu et al. 2019). Liu et al. (1998) studied the instability of the planar sheets by using linear stability analysis method theoretically. Their results suggested that the viscoelastic sheets tend to breakup more easily than the Newtonian sheets. Alleborn et al. (1999) described the viscoelastic of the annular liquid sheet by introducing an effective viscosity and concluded the annular liquid sheet was a general case by considering the limiting cases. The viscoelastic annular was more stable with an increasing axial tension in a co-flowing inviscid gas medium (Yang et al. 2013). The results of Fu et al. (2013) suggested that the liquid elasticity can enhance the instability of the gas-liquid interface.

It should be noted that the temperature difference between the gas passage and the liquid passage leads to heat and mass transfer between two phases, and it plays a significant role in determining the flow instability characteristics. Therefore, it is necessary to investigate the effects of heat and mass transfer. The effect of the heat and mass transfer on the gas-liquid interface was firstly considered in the study of Hsieh (1972), and he found that the instability of gas-liquid interface depends on the temperature difference between the vapor and the liquid. However, the Rayleigh-Taylor instability was weakened by heat and mass transfer (Hsieh 1977). Nayak and Chakraborty (1984) explored the K-H instability of a cylindrical gas-liquid interface with heat and mass transfer, and concluded that heat transfer has a destabilizing effect. Kim et al. (2008) carried out a linear viscous-irrotational analysis of the capillary instability with heat transfer and phase changes. They considered the cylindrical interface shared by two viscous incompressible fluids enclosed by two concentric cylinders. Different from the above studies, Mothanta et al. (2016) used viscous potential theory to study the linear temporal stability of coaxial confined jets in a vertical tube involving heat and mass transfer at the interface. And there were also many other literatures on the effect of the heat and mass transfer on the interface instability (Chawla

1975; Adham-Khodaparast et al. 1995; Asthana et al. 2014; Fu et al. 2017; Fu et al. 2018; Jia et al. 2019).

The studies cited above neglected the gas compressibility. It was reasonable when the gas velocity was much low than the local sound speed in some cases. However, the gas compressibility maybe a main factor for the breakup process and could not be neglected in such cases with high Mach number. Chen and Li (1999) studied a viscous liquid jet injecting into an inviscid compressible gas medium and concluded that the gas compressibility (especially at high Mach numbers) has a profound and significant influence on the stability of the liquid jet. Yan and Xie (2010) reported that the gas Mach number has a destabilizing effect. In addition, Li et al. (2019) found that neglecting the gas compressibility would result in the decrease of disturbance growth rate and dominant wavenumber for flow conditions with high gas Mach number, markedly underestimating the aerodynamic effects at the gas-liquid interfaces.

This study aims to investigate the temporal instability of confined swirling liquid film when the gas compressibility is considered. And the effects of mass and heat transfer and the liquid viscoelasticity on the instability at the gas-liquid interface are also taken into consideration. The dispersion curves are obtained by solving the dimensionless dispersion equation. The effect of dimensionless heat flux ratio between the evaporation heat flux and conduction heat flux is investigated. And effects of other dimensionless parameters on the instability of gas-liquid interface are also discussed.

2 Theoretical Framework

2.1 Problem Formulation

As shown in Fig.1, a viscoelastic liquid film is confined in a tube, with the compressible gas phase in the center. The liquid phase has a density of ρ_l , and temperature T_l . The gas phase is with a density ρ_g , and a temperature T_g . σ is the surface tension coefficient of liquid phase. The basic velocity components in the axial, radial and azimuthal directions for the liquid and gas phases are assumed to be $(\bar{U}_l, 0, \frac{A}{r})$ and $(\bar{U}_g, 0, 0)$, respectively, where $\frac{A}{r}$ is swirling velocity of the free swirling liquid film. It is assumed that the interface temperature is T_i , and the wall temperature is T_w . The gas phase is usually hotter than the liquid. Considering the gas compressibility, it is assumed that the gas density consists of basic and disturbance parts.

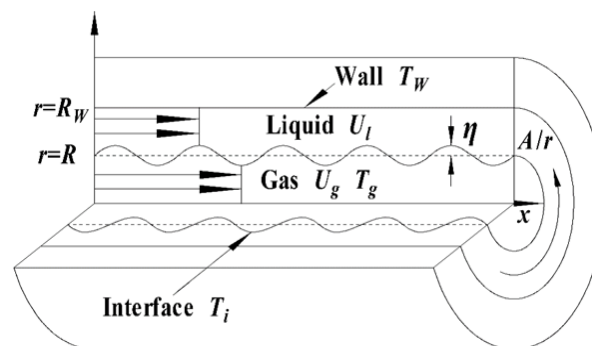


Fig. 1 Schematic of the profile of liquid jet.

According to the linear instability theory, the physical quantities are composed of basic and disturbed terms. The basic quantities remain unchanged with time and position, while the disturbed quantities vary both in time and space. In addition, the disturbances are assumed to be very small, so that the second- or higher-order terms can be ignored in the linearized equations.

The physical quantities can be expressed as follows

$$(U_j, V_j, W_j, P_j) = (\bar{U}_j, \bar{V}_j, \bar{W}_j, \bar{P}_j) + (u_j, v_j, w_j, p_j) \quad (1)$$

where $\bar{U}_j, \bar{V}_j, \bar{W}_j$ and \bar{P}_j are the basic velocity and pressure quantities, and u_j, v_j, w_j and p_j are the disturbed velocities and pressure quantities.

The perturbed velocity and pressure could be written in the normal mode as

$$\begin{aligned} (u_j, v_j, w_j, p_j) &= (\hat{u}_j, \hat{v}_j, \hat{w}_j, \hat{p}_j) \exp(\omega t + ikx + in\theta) \\ &= (\hat{u}_j, \hat{v}_j, \hat{w}_j, \hat{p}_j) \exp(\omega t + ikx + in\theta) \end{aligned} \quad (2)$$

where $\hat{}$ indicates the disturbance amplitude, and $j = l, g$ denotes liquid or gas. $i = \sqrt{-1}$ is the imaginary unit. $\omega = \omega_r + i\omega_i$ is complex frequency, the real part ω_r represents the temporal growth rate of the disturbance, and the imaginary part is related to the disturbance frequency. k is the wavenumber, related to the disturbance wavelength h by the relative expression $h = \frac{2\pi}{k}$. n is the azimuthal wavenumber. The displacement disturbance at the gas-liquid interface is:

$$\eta = \hat{\eta} \exp(\omega t + ikx + in\theta) \quad (3)$$

In present study, the viscoelasticity coefficient of liquid phase is λ , which can be ensured in the Oldroyd-B model. According to the previous studies (Fu et al. 2013, 2019; Liu et al. 1998; Alleborn et al. 1999; Yang et al. 2013), the viscoelastic coefficient can be ensured by the rheological equation of state, relating the stress tensor to the velocity field. The rheological equation is given by

$$\tau + \lambda_1 \begin{bmatrix} \frac{\partial \tau}{\partial t} + (v \cdot \nabla) \tau - (\nabla v)^T \cdot \tau \\ -\tau \cdot (\nabla v)^T \end{bmatrix} = \mu \left\{ \gamma + \lambda_2 \begin{bmatrix} \frac{\partial \gamma}{\partial t} + (v \cdot \nabla) \gamma - (\nabla v)^T \cdot \gamma \\ -\gamma \cdot (\nabla v)^T \end{bmatrix} \right\} \quad (4)$$

where λ_1 and λ_2 are two characteristic parameters of viscoelastic fluids, which denoting the stress relaxation time and deformation retardation time respectively. μ is the zero shear viscosity of liquid. τ is viscous stress tensor, v is velocity tensor of the viscoelastic liquid, and γ is the strain tensor. It should be noticed that the Oldroyd-B model can be reduced to the upper-convected Maxwell (UCM) model when $\lambda_1 \neq 0$ and $\lambda_2 = 0$. The expression of the viscoelastic coefficient obtained by linearized Eq. (4) is

$$\lambda = \mu \frac{1 + \left(\omega + ik\bar{U}_l + \frac{inA}{r} \right) \lambda_2}{1 + \left(\omega + ik\bar{U}_l + \frac{inA}{r} \right) \lambda_1} \quad (5)$$

2.2 Boundary Conditions

The boundary condition at $r \rightarrow 0$ is

$$v_g \rightarrow 0, r \rightarrow 0 \quad (6)$$

The boundary condition at the wall is

$$\frac{\partial \phi_l}{\partial r} = 0, r = R_w \quad (7)$$

The normal stress balance boundary condition at $r = R$ is

$$p_l - 2\lambda \frac{dv_l}{dr} + \frac{\rho_l A^2 \eta}{R^3} - p_g = \sigma \left(\frac{\eta}{R^2} + \frac{\partial^2 \eta}{\partial^2 x} + \frac{1}{R^2} \frac{\partial^2 \eta}{\partial \theta^2} \right), r = R \quad (8)$$

Because the mass flux of on either side of interface is the same, the linearized conservation equation of mass across the interface is given by (Hsieh 1972; 1977)

$$\bar{\rho}_g \left(v_g - \frac{\partial \eta}{\partial t} - \bar{U}_g \frac{\partial \eta}{\partial x} \right) = \rho_l \left(v_l - \frac{\partial \eta}{\partial t} - \bar{U}_l \frac{\partial \eta}{\partial x} \right), r = R \quad (9)$$

Eq. (9) is the mass transfer balance equation at the gas-liquid interface, and ρ_l represents the basic gas density. The heat transfer balance at the interface is expressed by

$$L\rho_l \left(v_l - \bar{U}_l \frac{\partial \eta}{\partial x} - \frac{\partial \eta}{\partial t} \right) = S(\eta) \quad (10)$$

where L is the released latent heat. As described by Hsieh (1972; 1977), $S(\eta)$ is the net heat flux at the interface when such a phase transformation is taking place. In general, the heat fluxes have to be resulted from equations governing the heat transfer in the fluids, thus completely coupling the dynamics and thermal exchanges in the entire flow region. In this simplified version, $S(\eta)$ is simply treated as a function of η , and to be determined from the heat exchange relation in the equilibrium state.

The heat absorbed by the evaporation is assumed to equal to the difference between the heat transported from inner gas to the interface and the heat transported from interface to the wall. In the present study, the heat transfer from the interface to the wall and the heat transfer from the interface to the liquid jet are treated as heat conduction and heat convection in the r direction, respectively. Thus, $S(\eta)$ could be written as

$$S(\eta) = \frac{k_g Nu(T_i - T_l)}{2(R + \eta)} + \frac{k_l(T_i - T_w)}{(R + \eta) \ln[R_w/(R + \eta)]} \quad (11)$$

where k_l and k_g denote the thermal conductivity of the liquid and gas, and $Nu = 2h_g(R + \eta)/k_g$ is the Nusselt number representing the ratio of heat conduction resistance to convective heat transfer resistance.

Eq. (11) is the nonlinear function of displacement disturbance η . To obtain the linearized heat flux equation, taking the Taylor series of Eq. (11) about gives

$$S(\eta) = S(0) + \eta S'(0) + \frac{1}{2} \eta^2 S''(0) + \dots \quad (12)$$

where $S(0)$ represents the net heat flux from the interface fluid region. The heat and mass transfer system is an equilibrium state (Hsieh 1972; 1977) when $\eta = 0$, so $S(0) = 0$ and $S(\eta) = \eta S'(0)$. Thus, we have that

$$S(0) = \frac{k_l(T_i - T_w)}{R \ln(R_w/R)} + \frac{k_g Nu(T_i - T_l)}{2R} = 0 \quad (13)$$

$$S'(\eta) = -\frac{k_g Nu(T_i - T_l)}{2(R + \eta)^2} - \frac{k_l(T_i - T_w)}{(R + \eta)^2 \ln[R_w/(R + \eta)]} + \frac{k_l(T_i - T_w)}{(R + \eta)^2 \ln^2[R_w/(R + \eta)]} \quad (14)$$

$$S'(0) = -\frac{k_l(T_i - T_w)}{R^2 \ln(R_w/R)} - \frac{k_g Nu(T_i - T_l)}{2R^2} + \frac{k_l(T_i - T_w)}{R^2 \ln^2(R_w/R)} = \frac{k_l(T_i - T_w)}{R^2 \ln^2(R_w/R)} \quad (15)$$

By choosing $\Delta T = T_w - T_i$, $\alpha = R_w/R$ and $\eta^* = \eta/R$, Eq. (12) can be written as

$$\overline{S(\eta^*)} = \frac{S(\eta)R}{\Delta T k_l} = \frac{k_g(T_i - T_l)Nu}{2k_l(1 + \eta^*)\Delta T} + \frac{1}{(1 + \eta^*) \ln[\alpha/(1 + \eta^*)]} \quad (16)$$

Expanding Eq. (16) at $r = R$, we obtain

$$\overline{S'(0)} = \frac{1}{\ln^2 \alpha} = \frac{1}{\bar{\Lambda}} \quad (17)$$

where $\bar{\Lambda} = k_l \Delta T / R^2$. Thus, $S(\eta) = \eta \bar{\Lambda} \overline{S'(0)}$. Moreover, the velocity disturbance of gas and liquid phase in r direction are

$$v_l = \left[\omega + ik\bar{U}_l + in \frac{A}{R^2} + \frac{\bar{\Lambda} \overline{S'(0)}}{\rho_l L} \right] \eta \quad (18)$$

$$v_g = \left[\omega + ik\bar{U}_g + \frac{\bar{\Lambda} \overline{S'(0)}}{\bar{\rho}_g L} \right] \eta \quad (19)$$

2.3 Theoretical Derivation

For the viscous liquid phase, the linearized continuity equation is

$$\nabla \cdot \mathbf{u}_l = 0 \quad (20)$$

where \mathbf{u}_l is the vector matrix and $\mathbf{u}_l = (u_l, v_l, w_l)$. Assuming that the perturbed liquid fluid motion is irrotational, the continuity equation is therefore can be expressed using the potential function φ_l

$$\mathbf{u}_l = \nabla \varphi_l \quad (21)$$

$$\nabla \cdot \mathbf{u}_l = \nabla^2 \varphi_l = 0 \quad (22)$$

where ∇^2 is Laplace operator and $\nabla^2 = \frac{\partial^2}{\partial r^2} + \frac{\partial}{r \partial r} + \frac{\partial^2}{r^2 \partial \theta^2} + \frac{\partial^2}{\partial x^2}$.

The solution of Eq. (22) is

$$\varphi_l = [A_1 I_n(kr) + A_2 K_n(kr)] \times \exp(\omega t + ikx + in\theta) \quad (23)$$

where A_1 and A_2 are undetermined coefficients, determined by boundary conditions; $I_n(kr)$ and $K_n(kr)$ are the n-order modified Bessel function of the first and second kind, respectively. After a complex mathematical derivation, the expression of potential φ_l is obtained as

$$\varphi_l = \frac{1}{k} \frac{I_n(kr)K'_n(kR_W) - I'_n(kR_W)K_n(kr)}{I'_n(kR)K'_n(kR_W) - I'_n(kR_W)K'_n(kR)} \times \left[\omega + ik\bar{U}_g + in \frac{A}{R^2} + \frac{\overline{\lambda S'(0)}}{\rho_l L} \right] \eta \quad (24)$$

According to the Bernoulli's equation, the pressure disturbance of confined swirling liquid film is

$$p_l = -\rho_l \left(\frac{\partial \varphi_l}{\partial t} + \bar{U}_l \frac{\partial \varphi_l}{\partial x} + \frac{A}{r^2} \frac{\partial \varphi_l}{\partial \theta} \right) \quad (25)$$

The linearized continuity and momentum equations of the compressible gas in potential flow theory are

$$\frac{\partial \hat{\rho}_g}{\partial t} + (\bar{U}_g \cdot \nabla) \hat{\rho}_g + \bar{\rho}_g \nabla^2 \varphi_g = 0 \quad (26)$$

$$\bar{\rho}_g \left(\frac{\partial}{\partial t} + \bar{U}_g \cdot \nabla \right) \nabla \varphi_g = -\nabla p_g \quad (27)$$

$$\left(\frac{\partial p_g}{\partial \rho_g} \right)_s = c^2 \quad (28)$$

where c is the local sound speed for the compressible gas. Substituting Eqs. (26) into Eq. (27), and utilizing the Eq. (28), the following linearized equation is obtained

$$\frac{1}{c^2} \left(\frac{\partial^2 p_g}{\partial t^2} + 2\bar{U}_g \frac{\partial^2 p_g}{\partial t \partial x} + \bar{U}_g^2 \frac{\partial^2 p_g}{\partial x^2} \right) = \nabla^2 p_g \quad (29)$$

The solution of Eq. (29) is

$$\hat{p}_g = B_1 I_n(qr) + B_2 K_n(qr) \quad (30)$$

where $q = \sqrt{k^2 + \frac{(\omega + ik\bar{U}_g)^2}{c^2}}$, B_1 and B_2 are coefficients which can be determined by boundary conditions. Taking Eq.(30) into Eq.(27) and utilizing the Eqs.(6) and (19), the expressions of B_1 and B_2 could be obtained as bellow

$$B_1 = -\frac{\bar{\rho}_g}{q} \frac{1}{I'(qR)} (\omega + ik\bar{U}_g) \times \left[\omega + ik\bar{U}_g + \frac{\overline{\lambda S'(0)}}{\bar{\rho}_g L} \right] \eta \quad (31)$$

$$B_2 = 0 \quad (32)$$

Taking solutions of φ_l and p_g into normal stress balance equation, then the dispersion equation is yielded

as

$$\begin{aligned}
 & -\frac{\rho_l I_n(kR)K_n'(kR_W) - I_n'(kR_W)K_n(kR)}{k I_n'(kR)K_n'(kR_W) - I_n'(kR_W)K_n'(kR)} \times \left(\omega + ik\bar{U}_l + in\frac{A}{R^2} \right) \times \left[\omega + ik\bar{U}_l + in\frac{A}{R^2} + \frac{\overline{\Lambda S'(0)}}{\rho_l L} \right] \\
 & - 2\lambda k \frac{I_n''(kR)K_n'(kR_W) - I_n'(kR_W)K_n''(kR)}{I_n'(kR)K_n'(kR_W) - I_n'(kR_W)K_n'(kR)} \times \left[\omega + ik\bar{U}_l + in\frac{A}{R^2} + \frac{\overline{\Lambda S'(0)}}{\rho_l L} \right] \\
 & + \frac{\bar{\rho}_g I_n(qR)}{q I_n'(qR)} (\omega + ik\bar{U}_g) \times \left[\omega + ik\bar{U}_g + \frac{\overline{\Lambda S'(0)}}{\bar{\rho}_g L} \right] = \frac{\sigma}{R^2} (1 - n^2 - k^2 R^2) - \frac{\rho_l A^2}{R^3}
 \end{aligned} \tag{33}$$

The final dispersion equation in non-dimensional form is

$$\begin{aligned}
 & -\frac{1}{K} \frac{I_n(K)K_n'(\alpha K) - I_n'(\alpha K)K_n(K)}{I_n'(K)K_n'(\alpha K) - I_n'(\alpha K)K_n'(K)} \times \left(\Omega + iK + \frac{in}{Ro} \right) \times \left(\Omega + iK + \frac{in}{Ro} + \frac{\overline{\Lambda S'(0)}}{Ro} \right) \\
 & - 2K\beta \frac{I_n''(K)K_n'(\alpha K) - I_n'(\alpha K)K_n''(K)}{I_n'(K)K_n'(\alpha K) - I_n'(\alpha K)K_n'(K)} \times \left(\Omega + iK + \frac{in}{Ro} + \frac{\overline{\Lambda S'(0)}}{Ro} \right) \\
 & + \frac{1}{Q} \frac{I_n(Q)}{I_n'(Q)} (\Omega + iK\gamma) \times \left[\Omega\rho + iK\rho\gamma + \overline{\Lambda S'(0)} \right] = \frac{1}{We} (1 - n^2 - K^2) - \frac{1}{Ro^2}
 \end{aligned} \tag{34}$$

where $R_W = \alpha R$ and $\alpha > 1$. The dimensionless wave number is $K = kR$, the dimensionless complex frequency is $\Omega = \frac{\omega R}{\bar{U}_l}$. The Reynolds number is $Re = \frac{\rho_l \bar{U}_l R}{\mu}$. The gas-liquid density ratio is $\rho = \frac{\bar{\rho}_g}{\rho_l}$. The Rossby

number is $Ro = U_l R/A$. The gas-liquid velocity ratio is $\gamma = \frac{\bar{U}_g}{\bar{U}_l}$. The liquid Weber number is $We = \frac{\rho_l \bar{U}_l^2 R}{\sigma}$.

The axial velocity and swirl velocity ratio of liquid phase is $Ro = \frac{R\bar{U}_l}{A}$. $\Lambda = \frac{\Delta T k_l}{(\rho_l \bar{U}_l L R)}$ represents the ratio

between conduction heat flux from the wall to the interface and the evaporation heat flux at the interface, where

$\Delta T = T_W - T_i$. $Q = \sqrt{Ma^2 \left(\frac{\Omega}{\gamma} + iK \right)^2 + K^2}$, and the gas Mach number $Ma = \frac{\bar{U}_g}{c}$. And $\beta =$

$\frac{[1+(\Omega+iK)]\Gamma_1}{Re[1+(\Omega+iK+\frac{in}{Ro})]}\Gamma_2$, the dimensionless stress relaxation time is $\Gamma_1 = \frac{\bar{U}_l \lambda_1}{R}$, and the dimensionless deformation

retardation time is $\Gamma_2 = \frac{\bar{U}_l \lambda_2}{R}$.

3 Results and discussion

If ignoring the liquid viscosity and gas compressibility, the reduced physical model is same to that of Fu et al. (2018), and the reduced dimensionless dispersion equation is

$$\begin{aligned}
 & -\frac{1}{K} \frac{I_n(K)K_n'(\alpha K) - I_n'(\alpha K)K_n(K)}{I_n'(K)K_n'(\alpha K) - I_n'(\alpha K)K_n'(K)} \times \left(\Omega + iK + \frac{in}{Ro} \right) \left(\Omega + iK + \frac{in}{Ro} + \frac{\overline{\Lambda S'(0)}}{Ro} \right) \\
 & + \frac{1}{K} \frac{I_n(K)}{I_n'(K)} (\Omega + iK\gamma) \times \left[\Omega\rho + iK\rho\gamma + \overline{\Lambda S'(0)} \right] = \frac{1}{We} (1 - n^2 - K^2) - \frac{1}{Ro^2}
 \end{aligned} \tag{35}$$

It should be noted that γ is gas-liquid velocity ratio in the present study while it is liquid-gas velocity ratio in the study of Fu et al. (2018). Figure 2 compares the results obtained by Eq. (35) with the those of Fu et al. (2018). Obviously, the results based on the present reducing dispersion relation agree well with those from Fu et al. (2018). This partially verifies the present dispersion relation. The growth rate curves are normal: the curves increase monotonously until the maximum growth rate, after which curves decrease and reach the axis of the abscissa. The presence of a maximum value is caused by the surface tension effects and viscous dissipation, and

the wavenumber corresponding to the maximum growth rate is called the dominant wavenumber. The unstable wavenumber range is from zero to the abscissa-crossing point. Furthermore, the maximum growth rate increases as Λ increases, while the unstable wavenumber range remains unchanged.

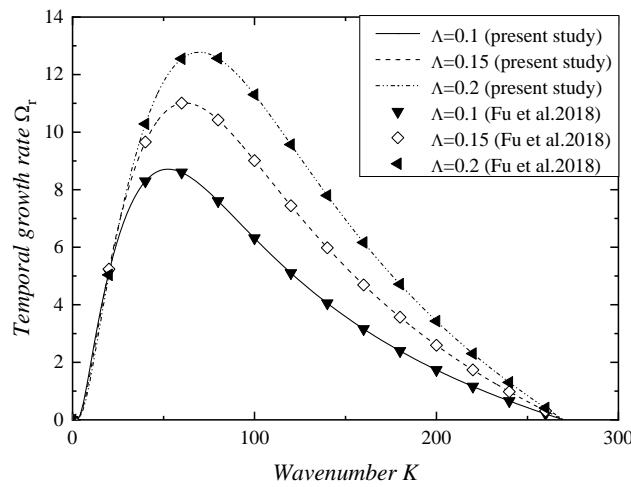


Fig. 2 Results compared with those of Fu et al. (2018) ($We=200$, $\gamma=10/3$, $\alpha=1.1$, $\rho=0.001$, $n=0$, $Ro=0.5$).

Figure 3 illustrates effects of Λ within the range 0.1-0.15, while other dimensionless parameters remain fixed. The maximum growth rate increases as Λ increases, implying that heat and mass transfer has a destabilizing effect on the gas-liquid interface. The distance between the gas-liquid interface and the wall decreases when the crest of gas-liquid interface increases. From the view of physical point, as the heat transfer across the interface is enhanced, evaporation is encouraged and the crest moves deeper into the liquid. As a result, the interface becomes unstable, similar to the results of Asthana et al. (2014). Further comparing Fig.2 and Fig. 3, the unstable region also increases with an increasing Λ when the liquid viscoelasticity and gas compressibility are considered. It should also be noted that the dominant wavenumber increases as Λ increases.

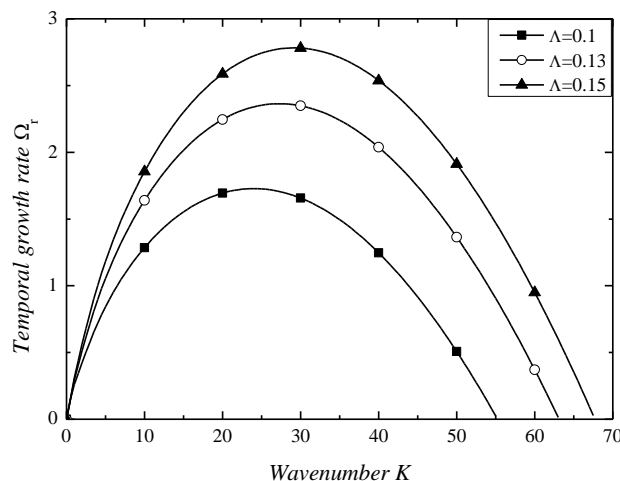


Fig. 3 Effects of Λ ($We=1000$, $Re=1000$, $\alpha=1.5$, $\rho=0.001$, $\gamma=5$, $Ma=0.3$, $n=0$, $Ro=0.5$, $\Gamma_1=1$, $\Gamma_2=1$).

As shown in Fig.4, both the unstable range and the maximum growth rate generally increase as the gas Mach number increases. It should be noted that temporal growth rate is nearly unchanged when the gas Mach number is smaller than 0.1. According to the final dispersion equation, the term $Q = \sqrt{Ma^2 \left(\frac{\Omega}{\gamma} + iK \right)^2 + K^2}$

denotes the effect of gas Mach number. When $Ma \ll 1$, $Q \approx K$. It predicts that the gas compressibility can be neglected when the gas velocity is much lower than the local sound velocity. However, the aerodynamic effect is enhanced obviously when the gas Mach number is high and increased. In such cases, the gas compressibility enhances disturbance growth rate, and promotes the liquid jet breakup processes. Moreover, the dominant wavenumber increases and the disturbance wavelength decreases as the gas Mach number increases.

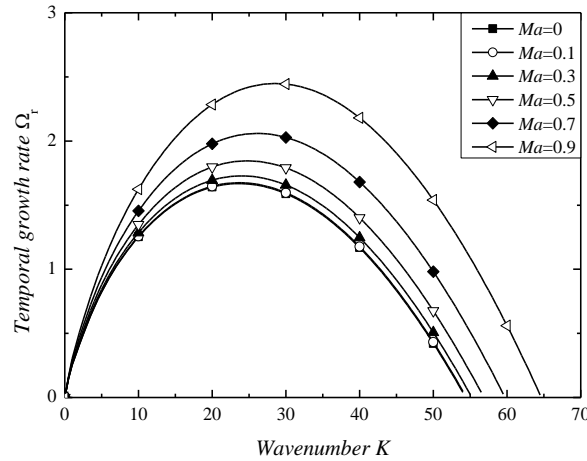


Fig. 4 Effects of the gas Mach number ($We=1000$, $Re=1000$, $\Lambda=0.1$, $\alpha=1.5$, $\rho=0.001$, $\gamma=5$, $Ro=0.5$, $n=0$, $\Gamma_1=1$, $\Gamma_2=1$).

Figure 5 shows the variation in the growth rate when the azimuthal wavenumber n varies from 0 to 7. The mode $n = 0$ represents the axisymmetric mode, and the modes $n \neq 0$ represents non-axisymmetric modes. Obviously, the mode $n = 0$ is most unstable, indicating that the gas-liquid interface tends to be more unstable in the axisymmetric mode than in the non-axisymmetric mode. According to the dispersion equation (i.e., Eq. (35)), the stabilizing effect of surface tension increases with an increasing azimuthal wavenumber n . Therefore, the mode $n = 0$ is more unstable than the modes $n \neq 0$.

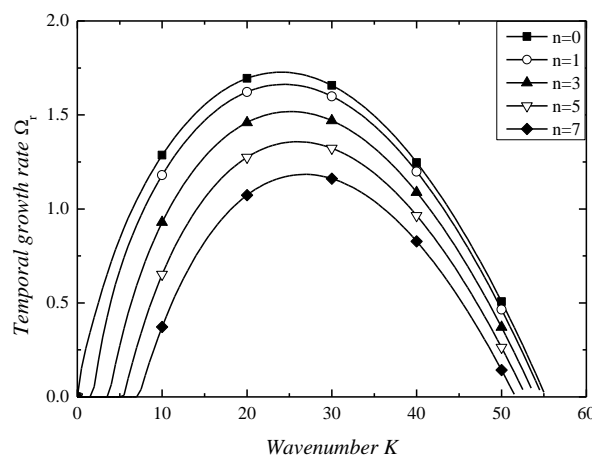


Fig. 5 Effects of azimuthal wavenumber ($We=1000$, $Re=1000$, $\Lambda=0.1$, $\gamma=5$, $\alpha=1.5$, $\rho=0.001$, $Ro=0.5$, $Ma=0.3$, $\Gamma_1=1$, $\Gamma_2=1$).

As displayed in Fig. 6, when increasing the Reynolds number, the maximum growth rate becomes larger, thus enhancing the gas-liquid interface instability. In addition, the dominant wavenumber increases with an

increasing Reynolds number. The Reynolds number is the ratio of the inertia force to the viscous force. When the viscous force decreases, or the inertia force increases, the Reynolds number would increase. The gas-liquid interface tends to be stable due to the damping effect of the viscous force. The results indicate that the weakening damping, the gas-liquid interface becomes unstable. Furthermore, both the unstable wavenumber range and the dominant wavenumber increase with an increasing Reynolds number. A larger wavenumber compresses a smaller wave length because of wavelength $\bar{h} = \frac{2\pi}{K}$. According to Aliseda et al. (2008; Qin et al. 2018; Fu et al. 2020; Yang et al. 2020), the short wavelength corresponds to the smaller droplets. Thus, the decrease of the liquid viscosity contributes to the atomizing fineness. It agrees with the tendency obtained by experimental results (Wang et al. 1987).

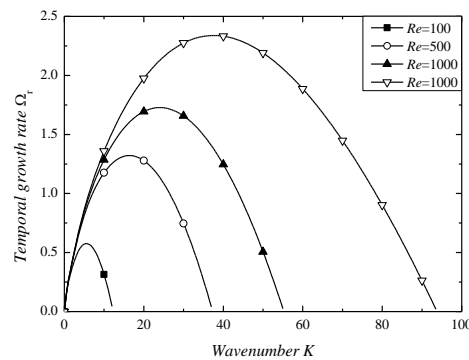


Fig. 6 Effects of Reynolds number ($We=1000$, $\Lambda=0.1$, $\alpha=1.5$, $\rho=0.001$, $\gamma=5$, $Ma=0.3$, $Ro=0.5$, $n=0$, $\Gamma1=1$, $\Gamma2=1$).

The effect of the Weber number is displayed in Fig. 7. The maximum growth rate, the unstable range, and the dominant wavenumber increase substantially when the Weber number increases. The Weber number is the ratio of inertia force to surface tension. The increase in the Weber number may be caused either by an increase in the axial velocity of the liquid layer or by decreasing the surface tension. For the K-H instability, dominated by the aerodynamic force, the surface tension plays a stabilizing role. In this case, the gas-liquid interface tends to be more unstable with a smaller the surface tension. The unstable range and the dominant wavenumber increase, i.e., the disturbance wavelength decreases, as the decrease of surface tension. Thus, it is benefiting to obtain smaller mean droplet size, which coincides well with the tendency pointed out by experiment results (Wang et al. 1987).

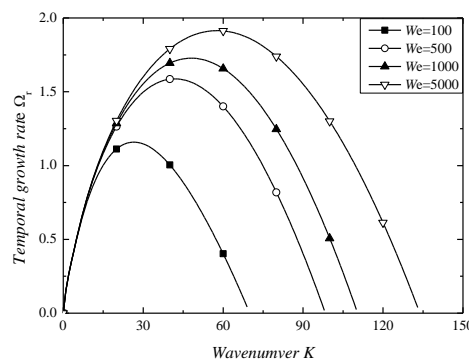


Fig. 7 Effects of Weber number with ($Re=1000$, $\Lambda=0.2$, $\alpha=1.5$, $\rho=0.001$, $\gamma=5$, $Ma=0.3$, $Ro=0.5$, $n=0$, $\Gamma1=1$, $\Gamma2=1$).

Figure 8 reveals the effect of the gas-liquid velocity ratio. Both the maximum growth rate and unstable range decrease as the gas-liquid velocity ratio decreases. This means that the instability of the confined viscous liquid film is enhanced with an increasing gas-liquid velocity ratio. For the flow with high velocity, the interface development is governed by the K-H instability. As the relative velocity between the liquid and gas phases increases, the aerodynamic forces would be stronger. Therefore, the gas-liquid interface gets more unstable. Furthermore, the increase of the gas-liquid velocity ratio results in an increase of the dominant wave number, i.e., the disturbance shifts to a short wavelength when the gas-liquid velocity ratio increases. According to recent studies (Aliseda et al. 2008; Qin et al. 2018; Fu et al. 2020; Yang et al. 2020), the short wavelength corresponds to the smaller droplets, thus, increasing the gas-liquid velocity ratio contributes to the better atomizing fineness.

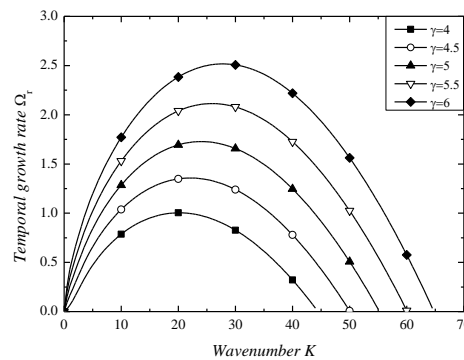


Fig. 8 Effect of gas-liquid velocity ratio γ ($We=1000$, $Re=1000$, $\Lambda=0.1$, $\alpha=1.5$, $\rho=0.001$, $Ma=0.3$, $Ro=0.5$, $n=0$, $\Gamma_1=1$, $\Gamma_2=1$).

Figure 9 reflects the effect of varying gas-liquid density ratio. As the gas-liquid density ratio ρ increases, both the maximum growth rate, and unstable range increase. It can be concluded that increasing gas-to-liquid density ratio enhances the interface instability. To put it physically, as the difference between the gas and liquid densities decreases, more momentum is imparted from the gas phase to the liquid phase, i.e., enhancing the aerodynamic interaction. As a result, the gas-liquid interface gets more unstable. This phenomenon is consistent with the classical K-H theory. In addition, the dominant wavenumber increases as the gas- liquid density ratio increases, which means that the disturbance wavelength decreases as the increase of gas-liquid density ratio increases.

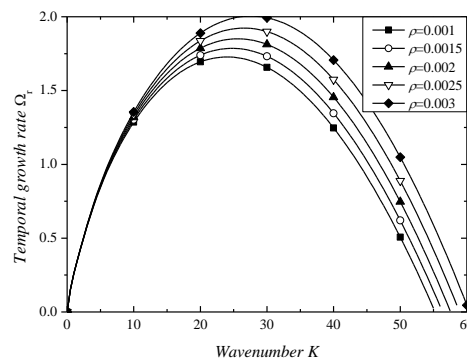


Fig. 9 Effects of gas-liquid density ratio ρ ($We=1000$, $Re=1000$, $\Lambda=0.1$, $\alpha=1.5$, $\gamma=5$, $Ma=0.3$, $Ro=0.5$, $n=0$, $\Gamma_1=1$, $\Gamma_2=1$).

$\alpha = \frac{R_W}{R}$ represents the relative thickness of the liquid and the gas phase. As shown in Fig. 10, the maximum growth rate decreases when α grows from 1.2 to 1.5. It means that the increase of the outer liquid phase has a stabilizing effect. When α increases, the thickness of outer liquid phase gets thicker and the inner gas phase gets relatively weaker. In this condition, the conduction heat transferring from the gas-liquid interface to the wall decreases (as shown in Eq. (17)), so that the amplitude of interface displacement decreases. Therefore, the gas-liquid interface gets stable. It is similar to the Fu et al. (2018).

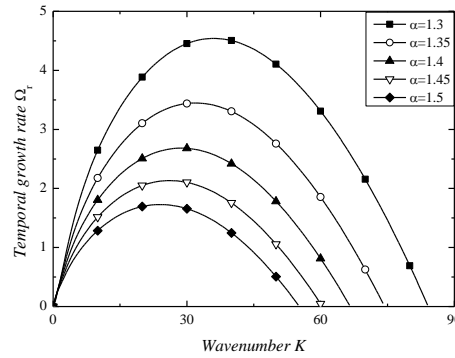


Fig. 10 Effects of α (We=1000, Re=1000, $\Lambda=0.1$, $\rho=0.001$, $\gamma=5$, Ma=0.3, Ro=0.5, n=0, $\Gamma_1=1$, $\Gamma_2=1$).

The effect of the dimensionless stress relaxation time on the instability of viscoelastic liquid film is further considered. As shown in Fig. 11, both the maximum growth rate and the range of the unstable wavenumber increases with an increasing dimensionless stress relaxation time, indicating that stress relaxation time has an unstable effect on the gas-liquid interface. The stress relaxation time represents the effect of liquid elasticity, the effect of liquid elasticity tends to increase the instability of the gas-liquid interface.

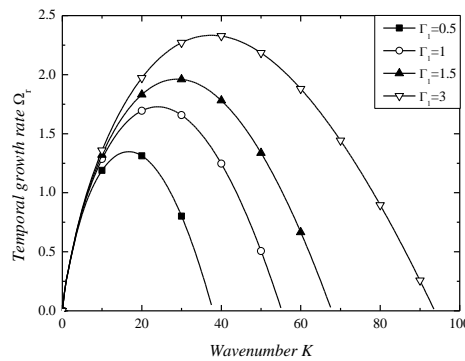


Fig. 11 Effects of dimensionless stress relaxation time (We=1000, Re=1000, $\Lambda=0.1$, $\alpha=1.5$, $\rho=0.001$, $\gamma=5$, Ma=0.3, Ro=0.5, n=0, $\Gamma_2=1$).

Figure 12 displays the influence of the dimensionless deformation retardation time on the instability of viscoelastic liquid film. As can be seen obvious in Fig. 12, when the dimensionless deformation retardation time increases, the maximum growth rate and stable region decreases, meaning that increasing deformation retardation time has a stabilizing effect on the gas-liquid interface. the stress tensor and dissipation of energy is increased with the increase of the deformation retardation time; therefore, the gas-liquid interface of the viscoelastic liquid film tends to be more stable with an increasing deformation retardation time.

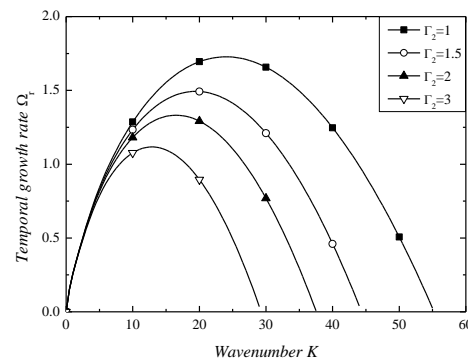


Fig. 12 Effects of the deformation retardation time ($We=1000$, $\Lambda=0.2$, $Re=1000$, $\alpha=1.2$, $\rho=0.001$, $\gamma=5$, $Ma=0.5$, $Ro=0.5$, $n=0$, $\Gamma_1=1$).

4 Conclusions

The linear temporal instability of a free swirling liquid film confined in a tube with central hotter gas is studied when considering heat and mass transfer. The liquid viscoelasticity and gas compressibility are also taken into consideration. The parametric discussion shows that the growth rate increases with an increasing the ratio of conduction heat flux to evaporation heat flux. However, different from the results for the cases ignoring the liquid the liquid viscosity and gas compressibility, the unstable wavenumber range also increases when the ratio of conduction heat flux to evaporation heat flux increases. Although increasing the gas Mach number could enhance the gas-liquid interface instability, both the growth rate and the unstable region are nearly unchanged when the gas Mach number is smaller than 0.1. Meanwhile, the increase of Weber number, gas-liquid density ratio and dimensionless stress relaxation time destabilizes the gas-liquid interface instability. The liquid film becomes more stable with an increasing α and dimensionless deformation retardation time. Furthermore, both maximum growth rate and the unstable range increase when the Reynolds number increases, while the increase of gas-liquid velocity ratio has an unstable effect.

Disclosure of Interests. The authors have no competing interests to declare that are relevant to the content of this article.

References:

- [1] Adham-Khodaparast, K., Kawaji, M. and B. Antar. The Rayleigh-Taylor and Kelvin-Helmholtz stability of a viscous liquid-vapor interface with heat and mass transfer. *Phys. Fluids* 7(2), 359-364 (1995)
- [2] Aliseda, A., E.J. Hopfinger, J.C. Lasheras, D.M. Kremer, A. Berchielli and E.K. Connolly, Atomization of viscous and non-newtonian liquids by a coaxial, high-speed gas jet. *Experiments and droplet size modeling*, *Int. J. Multiphase Flow* 34(2), 161-175 (2008)
- [3] Alleborn N., H. Raszillier and F. Durst. Linear stability of non-Newtonian annular liquid sheets, *Acta Mech.* 137, 33-42 (1999)
- [4] Asthana, R., M.K. Awasthi and G.S. Agrawal. Viscous correction for viscous potential flow analysis of Kelvin-Helmholtz instability of a cylindrical flow with heat and mass transfer. *Int. J. Heat Mass Transfer* 78(23), 251-259 (2014)
- [5] Chawla, T.C.. The Kelvin-Helmholtz instability of the gas-liquid interface of a sonic gas jet submerged in a liquid, *J. Fluid Mech.* 67(3), 513-537 (1975)
- [6] Chen T.B., X.G. Li, Liquid Jet Atomization in a Compressible Gas Stream, *J. Propulsion and Power* 15 (3) 369-376 (1999)

- [7] Dharmendra, S.T., and Gaurav Sharma. Manipulation and control of instabilities for surfactant-laden liquid film flowing down an inclined plane using a deformable solid layer, *Phys. Fluids* 30, 014104 (2018)
- [8] ZHANG Botao,Zhang Youping,ZHANG Minqing.High-precision numerical simulation of breakup processes of liquid jet in incompressible airflow[J].*Journal of Rocket Propulsion*, 44(01):59-66 (2018)
- [9] Eggers, J. and E. Villermaux. Physics of liquid jets, *Rep Prog Phys* 71(3), 37-51 (2008).
- [10] Fu, Q.F., X.D. Deng, B.Q. Jia and L.J. Yang. Temporal Instability of a Confined Liquid Film with Heat and Mass Transfer, *AIAA J.* 56(7), 2615-2622 (2018)
- [11] Fu, Q.F., X.D. Deng and L.J. Yang. Kelvin-Helmholtz instability of confined Oldroyd-B liquid film with heat and mass transfer, *J. Non-Newton Fluid Mech.* 267, 28-34 (2019)
- [12] Fu, Q.F., B.Q. Jia, L.J. Yang. Stability of a confined swirling annular liquid layer with heat and mass transfer, *Int. J. Heat Mass Transfer* 104, 644-649 (2017)
- [13] Fu, Q.F., L.J. Yang, P.M. Chen, Y.X. Liu, C. Wang. Spatial-Temporal Stability of an Electrified Viscoelastic Liquid Jet, *J. Fluid Eng.-T. ASME* 135(9), 094501 (2013)
- [14] Fu, Q.F., M.W. Yao, L.J. Yang and L. Xie (2020). Atomization Model of Liquid Jets Exposed to Subsonic Crossflows, *AIAA J.* 58, 1-5 (2020)
- [15] Funada, T., D.D., Joseph. Viscous potential flow analysis of Kelvin-Helmholtz instability in a channel, *J. Fluid Mech.* 445, 263-283 (2001)
- [16] Funada, T., and D.D. , Joseph, Yamashita S., Stability of a liquid jet into incompressible gases and liquids, *Int. J. Multiphase Flow* 30 (11), 1279-1310 (2004)
- [17] Hsieh D.Y. . Effects of Heat and Mass Transfer on Rayleigh-Taylor Instability, *J. Fluids Eng-Trans. ASME* 94 (1), 156-160 (1972)
- [18] Hsieh D.Y. . Interfacial stability with mass and heat transfer, *Phys Fluids* 21(5), 745-748 (1977)
- [19] Hu K.X., M. He and Q.S. Chen. Instability of thermocapillary liquid layers for Oldroyd-B fluid, *Phys. Fluids* 28, 033105 (2016)
- [20] Hu, K.X., M. He, Q.S. Chen, R. Liu. Linear stability of thermocapillary liquid layers of a shear-thinning fluid, *Phys. Fluids* 29, 073101 (2017)
- [21] Hu, K.X., M. He, Q.S. Chen. Thermocapillary instabilities of liquid layers on an inclined plane, *Phys. Fluids* 30, 082101 (2018)
- [22] YANG Guohua, ZHANG Botao, ZHOU Lixin,et al. Effects of momentum ratio on atomization characteristics of internal mixing gas-liquid injector[J].*Journal of Rocket Propulsion*, 45(05):66-73 ,(2019)
- [23] Hu, T., Q.F. Fu and L.J. Yang. Falling film with insoluble surfactants: effects of surfacelastcity and surface viscosities, *J. Fluid Mech.* 889, A16. (2020)
- [24] Jia B.Q., L. Xie, X. Cui, L.J. Yang and Q.F. Fu. Linear stability of confined coaxial jets in the presence of gas velocity oscillations with heat and mass transfer, *Phys Fluids* 31, 092101 (2019)
- [25] Joseph, D.D., T. Funada and J. Wang, *Potential flows of viscous and viscoelastic fluids*, Cambridge University Press, New York. (2008)
- [26] Kim, H.J., S.J. Kwon, J.C. Padrino and T. Funada. Viscous potential flow analysis of capillary instability with heat and mass transfer, *J. Phys. A-Math. Theor.* 41 (33), 1-11 (2008)
- [27] Lafrance, P. Nonlinear breakup of a laminar liquid jet, *Phys Fluids* 18 (4) 428-432 (1975)
- [28] Li, G.B., Y.R. Wang and L.M. Xiao. Instability of an annular liquid sheet exposed to compressible gas flows, *Int. J. Multiphas*

- flow 119, 72-83 (2019)
- [29] Li, X.G. . Mechanism of atomization of a liquid jet, *Atomization Spray* 66 (1), 113-120 (1995)
- [30] Liu Z., G. Brenn, F. Durst. Linear analysis of the instability of two dimensional non-Newtonian liquid sheet, *J. Non-Newton. Fluid Mech.* 78, 133-166 (1998)
- [31] Mohanta, L., F.B. Cheung, S.M. Bajorek. Stability of coaxial jets confined in a tube with heat and mass transfer, *Physica A* 443, 333-346 (2016)
- [32] Nayak, A.R., B.B. Chakraborty, Kelvin-Helmholtz stability with mass and heat transfer. *Phys. Fluids* 27 (8), 1937-1941 (1984)
- [33] Qin L.Z., R. Yi and L.J. Yang. Theoretical breakup model in the planar liquid sheets exposed to high-speed gas and droplet size prediction, *Int. J. Multiphase Flow* 98, 158-167 (2018)
- [34] Rayleigh, L. . On the instability of jets, *Proc. Lond. Math. Soc.* 10 (1) 4-13 (1878)
- [35] Reitz, R.D. and F.V. Bracco. Mechanism of atomization of liquid jet, *Phys Fluids* 25 (10) 1730-1742 (1982)
- [36] Wang, J., Joseph D.D., Funada T. . Viscous contributions to the pressure for potential flow analysis of capillary instability of viscous fluids, *Phys. Fluids* 17 (052105), 1-12 (2005)
- [37] Wang, X.F. and A.H. Lefebvre. Mean Drop Sizes from Pressure-Swirl Nozzles. *J. Propuls Power* 3 (1), 11-18 (1987)
- [38] Yang, L.J., Gao Y.P., J.X. Li and Q.F. Fu. Theoretical atomization model of a coaxial gas-liquid jet, *Phys Fluids* 32, 124108 (2020)
- [39] Yan, C. and Xie M. . Stability of an annular viscous liquid jet in compressible gases with different properties inside and outside of the jet, *Front. Energy Power Eng. China* 4, 198-204 (2010)
- [40] Yang, L.J., Tong M.X., Q.F. Fu. Instability of viscoelastic annular liquid sheets subjected to unrelaxed axial elastic tension, *J. Non-Newton. Fluid Mech.* 198, 31-38 (2013)